V European Conference on Computational Fluid Dynamics
ECCOMAS CFD 2010
J. C. F. Pereira and A. Sequeira (Eds)
Lisbon, Portugal, 14–17 June 2010

COMPUTATIONAL ANALYSIS OF AEROACOUSTIC WAVES INDUCED BY ROTATING TIRE

Ittetsu Kaneda[*], Taku Nonomura[†], Kozo Fujii[†],

Toshiyuki Ikeda[††] and Masataka Koishi[††]

[*]University of Tokyo
3-1-1 Yoshinodai Sagamihara Kanagawa 229-8510, Japan
e-mail: kaneda@flab.isas.jaxa.jp

[†]Institute of Space and Astronautical Science, JAXA
3-1-1 Yoshinodai Sagamihara Kanagawa 229-8510, Japan

[††]The Yokohama Rubber Corporation
2-1 Oiwake Hiratsuka Kanagawa 254-8601, Japan

Key words: tire, pattern, noise, aeroacoustic, simulation, CFD, LES

Abstract. *It is known that acoustic waves of more than 1000Hz are generated from the tire pattern, and one possibility of their generation mechanism is aeroacoustic effect. The aim of this research is to clarifiy the aeroacoustic effect on this phenomenon with computational fluid dynamics and aeroacoustics. The flow and acoustic fields around rotating tire are simulated with large eddy simulation (LES), whereas freestream Mach number is 0.1, Reynolds number is* 1×10^4 *based on the freestream velocity and tire diameter. The sixth-order compact difference scheme is used for the spatial difference. For the time integration, the second-order backward difference scheme converged by alternate directional implicit-symmetric Gauss-Seidel (ADI-SGS) scheme with three sub-iterations is used. Two cases, without-pattern case and longitudinal-pattern case are computed to investigate the effects of the pattern of tire. The result shows that the rear region of tire has the strong pressure fluctuation which is considered as the effect of longitudinal-pattern and that acoustic waves are generated from the rear region of tire at the frequencies of 690~1380Hz.*

1 INTRODUCTION

As the noises from engine of automobile are reduced recently, those from tire increase relatively. Noises generated from tire-pattern are of strong interest for creating new models of a tire. It is known that acoustic waves of more than 1000Hz are generated from the tire pattern[1], and they are possibly generated by aeroacoustic effect. However, it is difficult to identify the aeroacoustic wave sources by the experiment because a tire is rotating and the vibroacoustic wave sources might exist.[1]

Now, computational fluid dynamics (CFD) and computational aeroacoustics (CAA) are developed and used for various practical simulations. Using CFD or CAA, aeroacoustic wave sources of a rotating tire can be analyzed without considering effects of vibroacoustic waves. The objective of this research is to clarify the aeroacoustic effect on this phenomenon with computational fluid dynamics and aeroacoustics.

In this paper, experimental condition is simulated in which a tire and ground is moving, but freesrteam is not imposed. Two cases, without-pattern case and with tire pattern case, are computed and aeroacoustic effects of tire pattern are discussed. In section 2, the computational setup is described. In section 3, the result and discussion are presented. In section 4, this paper is concluded.

2 COMPUTATIONAL SETUP

2.1 Problem settings

In this paper, experimental condition is simulated in which tire and ground is moving, but freesream is not imposed. The Mach number based on rotating speed of a tire is set to 0.1, Reynolds number based on the tire rotating speed and diameter is set to 1×10^4. Reynolds number of the experimental condition of tire (122 km/hour) is approximately 1×10^6, but it is impossible to calculate such a high Reynolds number condition with accurate large-eddy simulation (LES) adopted in this study because of very large number of grid points. Thus, lower Reynolds number is intentionally used for accurate LES. Although condition analyzed in this research is different from that in real experiments due to intentionally selected low Reynolds number, it does not seems to matter to understand phenomenon qualitatively. In this study, two cases, without-pattern case and longitudinal-pattern case, are computed to investigate the effects of tire pattern.

2.2 Computational method

The governing equations are three-dimensional compressible Navier-Stokes equations. Length, density, and velocity are nondimensionalized by the diameter of tire, density, and speed of sound for the ambient condition, respectively. The computational code used here is based on the well-validated Navier-Stokes code with the recent modifications of more efficient implicit time integration scheme and high-order accurate evaluation of space derivatives. Sixth-order central difference scheme[2,3] is employed for the spatial difference. For the time integration, the second-order backward difference scheme converged by ADI-SGS scheme with three sub-iterations is used. ILES is conducted, thus no sub-grid scale model is used. The rotation of tire is presented by the moving-wall boundary condition whereas the fixed grid is employed.

2.3 Computational grids and time steps

The purpose of this analysis is to understand flow physics at the region where tire connect to ground. Generally, in the case of analysis with structured meshes, a part of grid is located underground as shown in Figure 1 left. However, this method reduces accuracy for interpolation around the point where a tire connects to ground.

To improve the accuracy of the point where tire connect to ground, a punctured mesh is employed in this study as shown in Figure 1 right. This method makes stability of analysis bad because of reducing grid size unnecessarily, but enables us to improve accuracy of flow around the region where a tire connects to ground and to satisfy conservation law better.

Computational grid is shown in Figures 2 and 3. Acoustic waves are resolved by a tire grid (black zone) and a background grid (red zone), and buffer region is set at the outside of a background grid for avoiding non-physical wave emissions and reflections. Also, a grid for pattern is shown in Figure 4.

Number of tire grid is 186 x 201 x 91, number of background is 165 x 133 x 144, and number of longitudinal-pattern grid is 186 x 21 x 36. Thus, total number of grid point is approximately 6.5 million in without-pattern case and 6.7 million in longitudinal-pattern case. The time steps in without-pattern case and longitudinal-pattern case is 0.005 and 120,000 steps in total are integrated for the discussion of both cases. Thus, total time of integrations is 600.

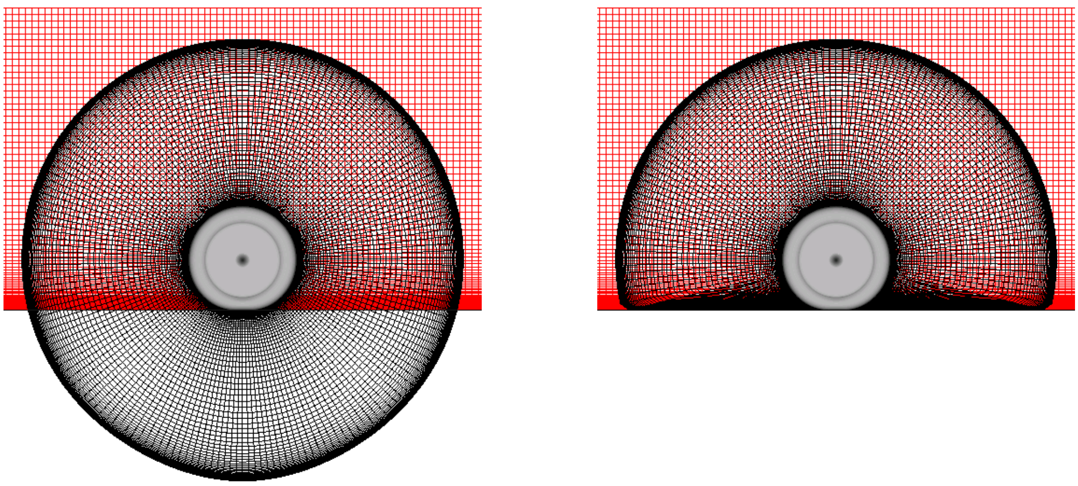

Figure 1:Schematic of grid types (left:tire grid gone underground, right: punctured tire grid, black zone: tire grid, red zone: background grid)

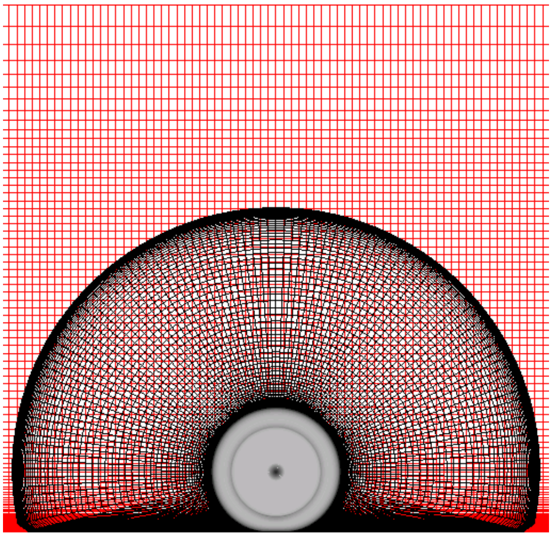

Figure 2:Calculation grid(side view, black zone:tire grid, red zone:background grid)

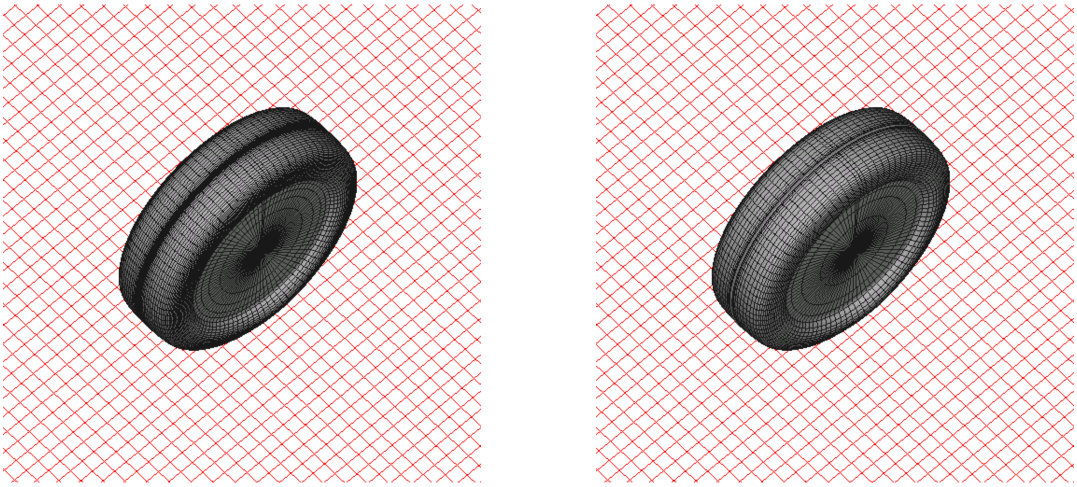

Figure 3:Calculation grid(air view, black zone:tire grid, red zone:background grid)

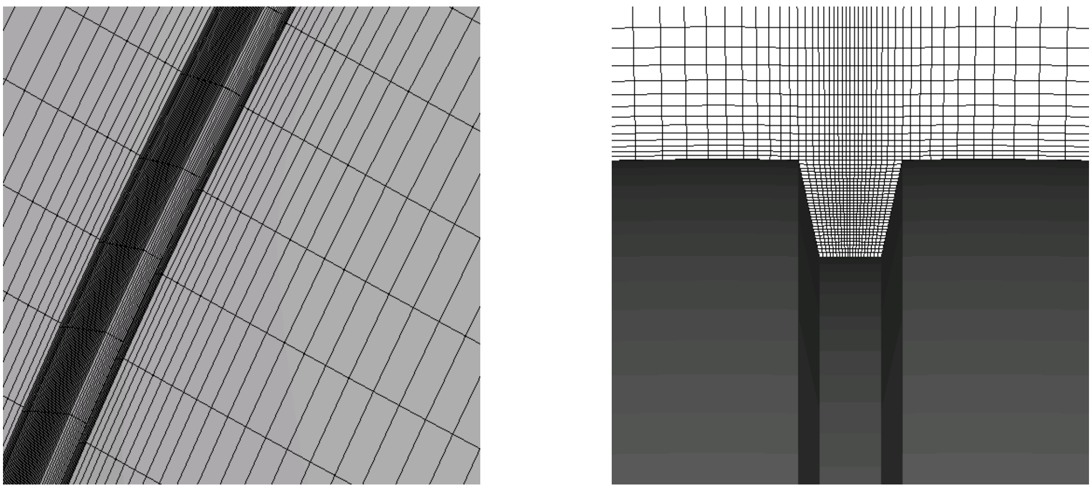

Figure 4:Pattern grid

3 RESULTS AND DISCUSSIONS

3.1 Flow field

Flow field is discussed in this subsection. Averaged pressure distribution is shown in Figures 5 and 6, and averaged pressure distributions with streamline on the cross section are shown in Figures 7 and 8. Figures 7 and 8 shows that flow entrained by tire rotation collides at forward bottom wall, resulting in high pressure region shown in Figure 5. Moreover, entrained flow also makes low pressure region at the rear region where a tire is detaching from the ground, as shown in Figure 6. Averaged flow fields of without-pattern case and longitudinal-pattern case are almost the same. Instantaneous pressure distribution and vortex structure (Iso-surfaces of 2nd invariant of the velocity gradient tensors) are shown in Figures 9 and 10. Figures 9 and 10 show that instantaneous flow fields of without-pattern case and longitudinal-pattern case are also almost the same, and the instantaneous fluctuation is small compared with averaged flow fields. Also, vortex structures of without-pattern case and longitudinal-pattern case are almost the same.

In Figure 5, the oscillation of pressure is shown around the space enclosed by dashed-line. This has prospects of numerical oscillation because this low Mach number condition might be near the limit of compressible solver, and pressure changes easily by grid distortions. In order to control such oscillation, it is necessary to make a better grid in terms of skewness or stretching, but it is difficult because punctured tire grid is adopted in this study.

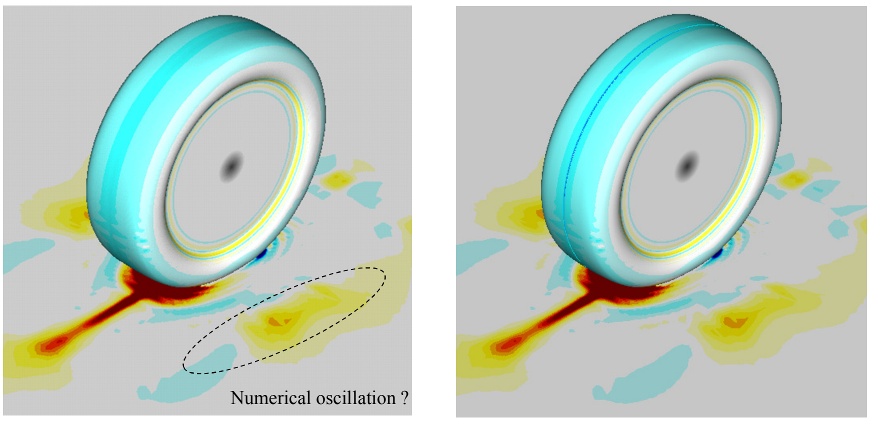

(a)Without-pattern (b)Longitudinal-pattern

Figure 5:Average pressure distribution(fore air view)

contor: nodimensional pressure 0.999~1.001

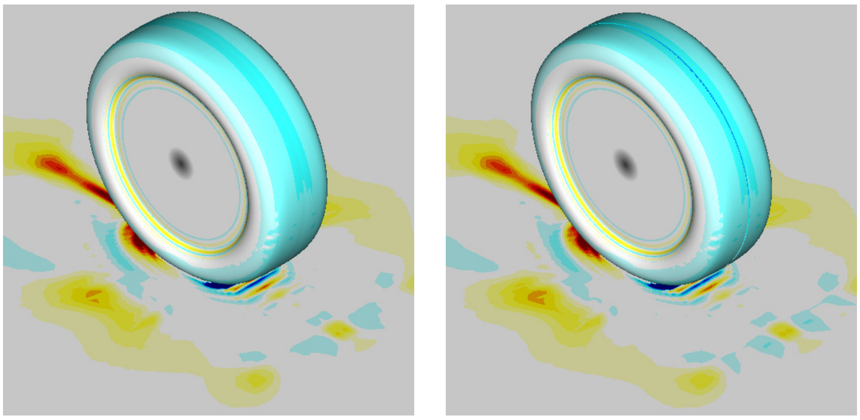

(a)Without-pattern (b)Longitudinal-pattern

Figure 6:Average pressure distribution(rear air view)

contor: nondimensional pressure 0.999~1.001

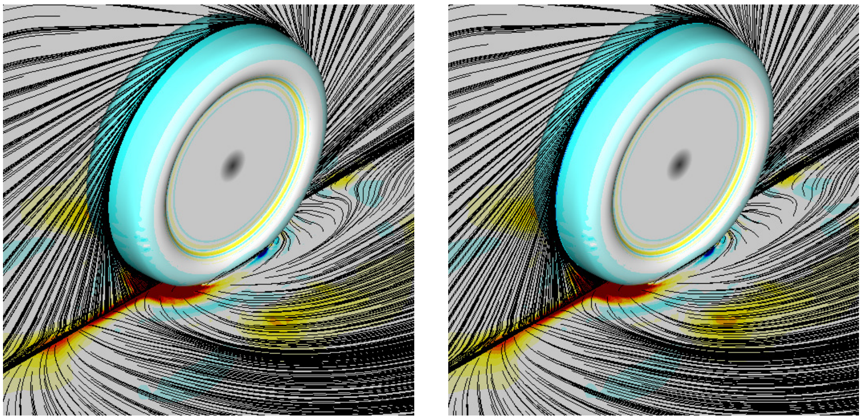

(a) Without-pattern (b)Longitudinal-pattern

Figure 7: Average pressure distribution with streamline on the cross section of space(fore air view)

Contor: nodimensional pressure 0.999~1.001

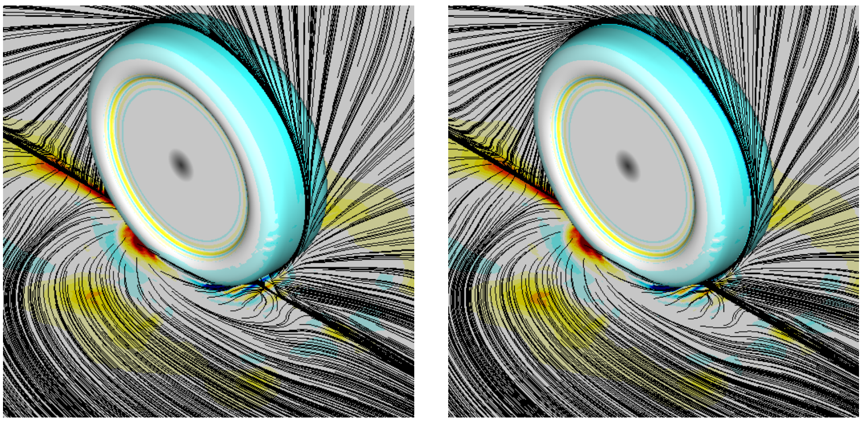

(a) Without-pattern (b)Longitudinal-pattern

Figure 8: Average pressure distribution with streamline on the cross section of space(rear air view)

contor: nondimensional pressure 0.999~1.001

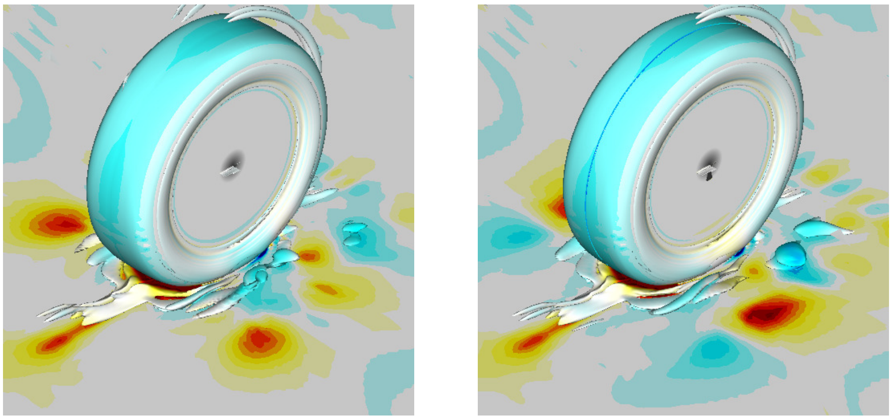

(a) Without-pattern (b)Longitudinal-pattern

Figure 9: Instantaneous pressure distribution and Iso-surfaces of 2nd invariant of the velocity gradient tensors (side view)

Iso-surfaces of 0.5

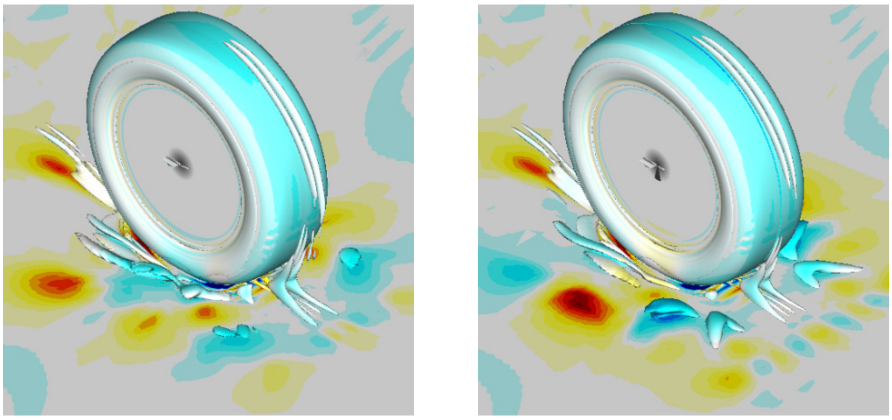

(a) Without-pattern (b)Longitudinal-pattern

Figure 10: Instantaneous pressure distribution and Iso-surfaces of 2nd invariant of the velocity gradient tensors (side view)

Iso-surfaces of 0.5

3.2 Acoustic field

Octave band-filtered sound-pressure-level distributions are shown in Figure 10 and 11. The results of frequency of less than 172Hz are not shown because the acoustic waves generated in this range are not of interest in this study. Also, the results of frequency of more than 1300Hz are not shown because sound pressure level cannot be estimated due to lack of grid resolution. As shown in Figure 10(a) and 11(a), circles in the result of 345Hz shows numerical oscillations because of distortions of grid and interpolation for different grid zones. Except for these oscillations, SPL seems to be well-captured. From sound pressure level in frequency of more than 690Hz, high sound pressure level area is observed at the rear tire part for longitudinal-pattern. Although physical mechanism of sound source is not clarified because the flow field are almost same , there is a possibility that the longitudinal-pattern makes high frequency turbulent disturbances at rear tire area and acoustic waves are generated from the region. Furthermore, it turns out that the sound pressure level in front of tire for without-pattern case is higher than that of longitudinal-pattern case from the sound-pressure-level field of 690Hz(Figure 10(b) and 11(b)).

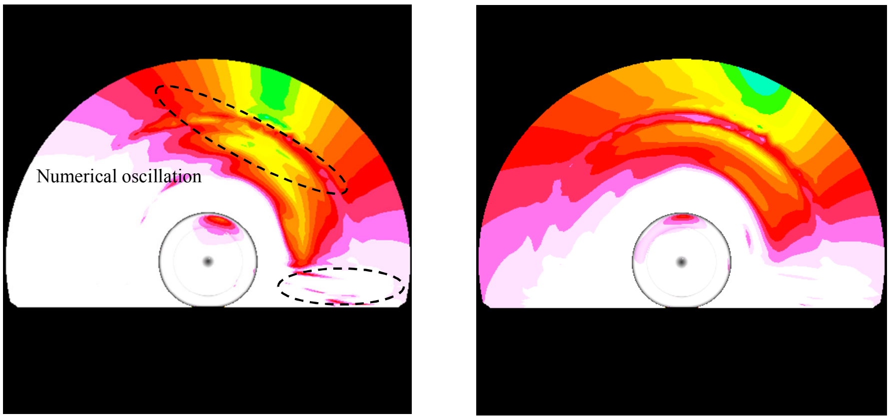

(a)St=6.4~*f*=345Hz

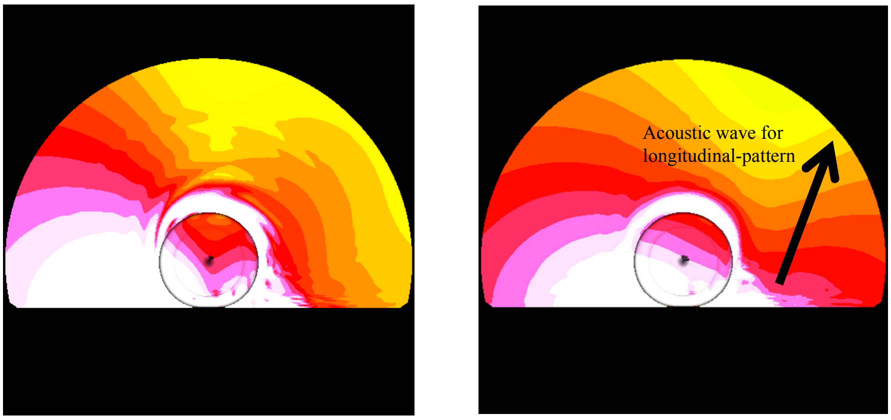

(b)St=12.8~*f*=690Hz

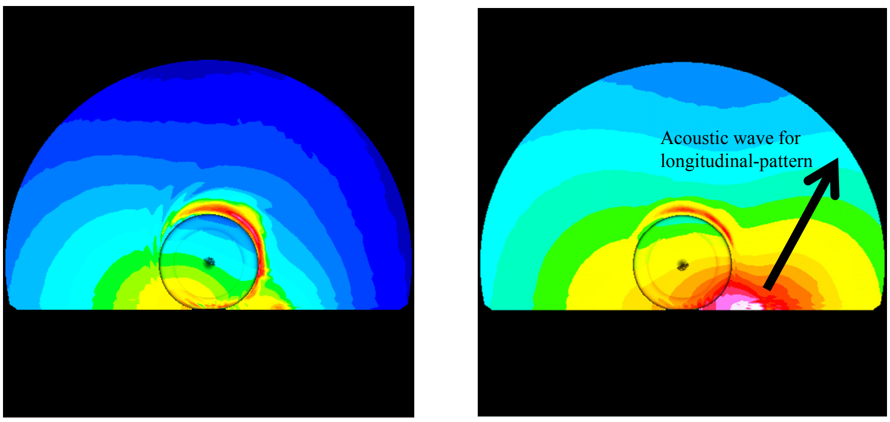

(c)St=25.6~*f*=1381Hz

Figure 10:Sound pressure level on the symmetry plane and tire surface(octave band)

left:without-pattern right:Longitudial pattern contor:40~80dB

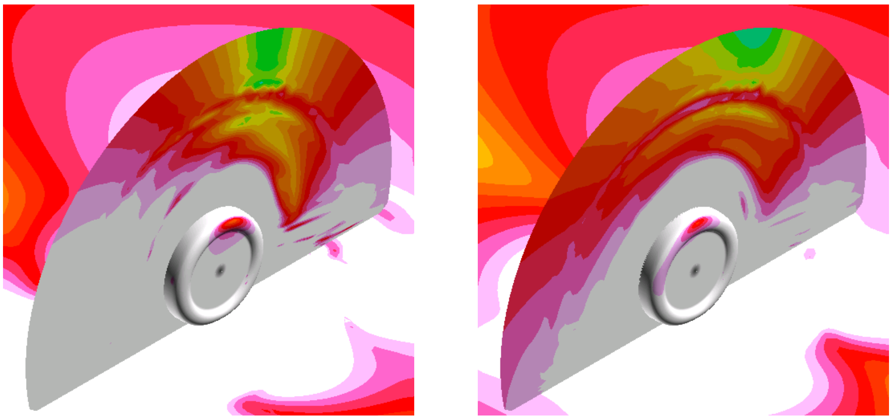

(a)St=6.4~*f*=345Hz

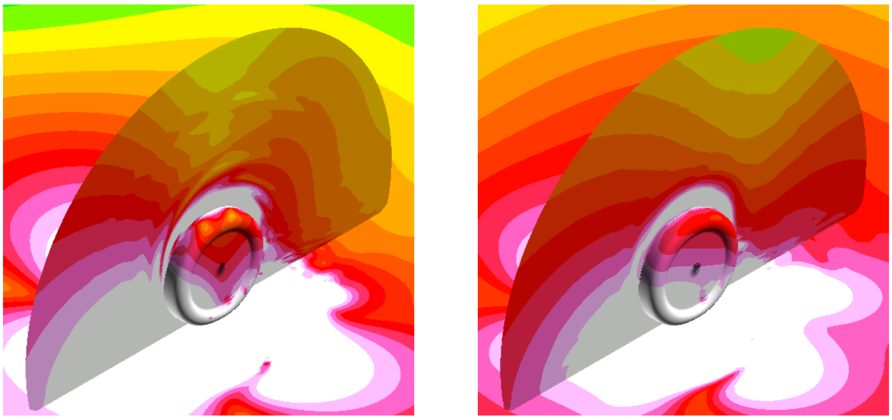

(b)St=12.8~*f*=690Hz

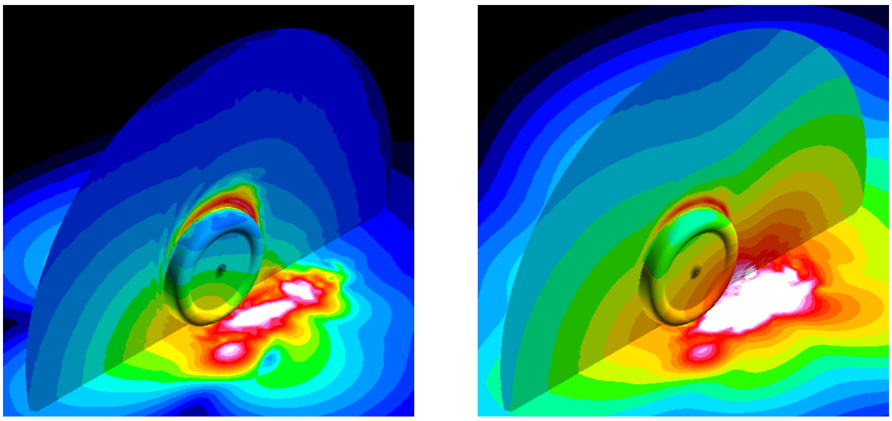

(c)St=25.6~*f*=1381Hz

Figure 11:Sound pressure level on the ground and tire surface(octave band)

left:without-pattern right:Longitudial pattern

contor:40~80dB

4 CONCLUSIONS

Effects of pattern on the tire are investigated by CAA/CFD. Without-pattern case and longitudinal-pattern case are computed and the results are discussed. In flow fields, without-pattern case and longitudinal-pattern case are almost the same. In the acoustic fields of the frequencies between 690Hz and 1380Hz, the rear tire region has strong pressure fluctuation which is considered as the effect of longitudinal-pattern, and acoustic waves generated from the region are observed. Though the numerical oscillation due to both grid distortions and low Mach number conditions are observed, the results qualitatively show that aeroacoustic waves seems to be generated by the tire pattern at the rear tire region.

REFERENCES

[1] PERISSE J. ; CLAIRET J. M. ; HAMET J. F. , Modal testing of a smooth tire in low and medium frequency- estimation of structural parameters , International modal analysis conference N°18, San Antonio TX, ETATS-UNIS 2000, vol. 4062(2), pp.960-967

[2] Lele, S.K., “Compact finite difference scheme with spectral-like resolution,” Journal of Computational Physics, Vol.103, pp.16-22 (1992).

[3] Visbal, M.R., and Rizzetta, D.P., “Large-eddy simulation on general geometries using compact differencing and filtering schemes,” AIAA Paper 2002-288, AIAA Aerospace Sciences Meeting and Exhibit, 40th, Reno, NV, Jan. 14-17 (2002).